Supplementary Information

Non-Solvent Induced Phase Inversion Strategy Enables Scaling Resistance Without Post-Modification for Membrane Distillation Application

Joel Parayil Jacob[a] and Raju Kumar Gupta[a,b,c,d*]

[a] Department of Chemical Engineering, Indian Institute of Technology Kanpur, Kanpur, 208016, India

[b] Department of Sustainable Energy Engineering, Indian Institute of Technology Kanpur, Kanpur, 208016, India

[c] Chandrakanta Kesavan Centre for Energy Policy and Climate Solutions, Indian Institute of Technology Kanpur, Kanpur, 208016, India

[d] Kotak School of Sustainability, Indian Institute of Technology Kanpur, Kanpur, 208016, India

*Corresponding author Email: guptark@iitk.ac.in (Raju Kumar Gupta)

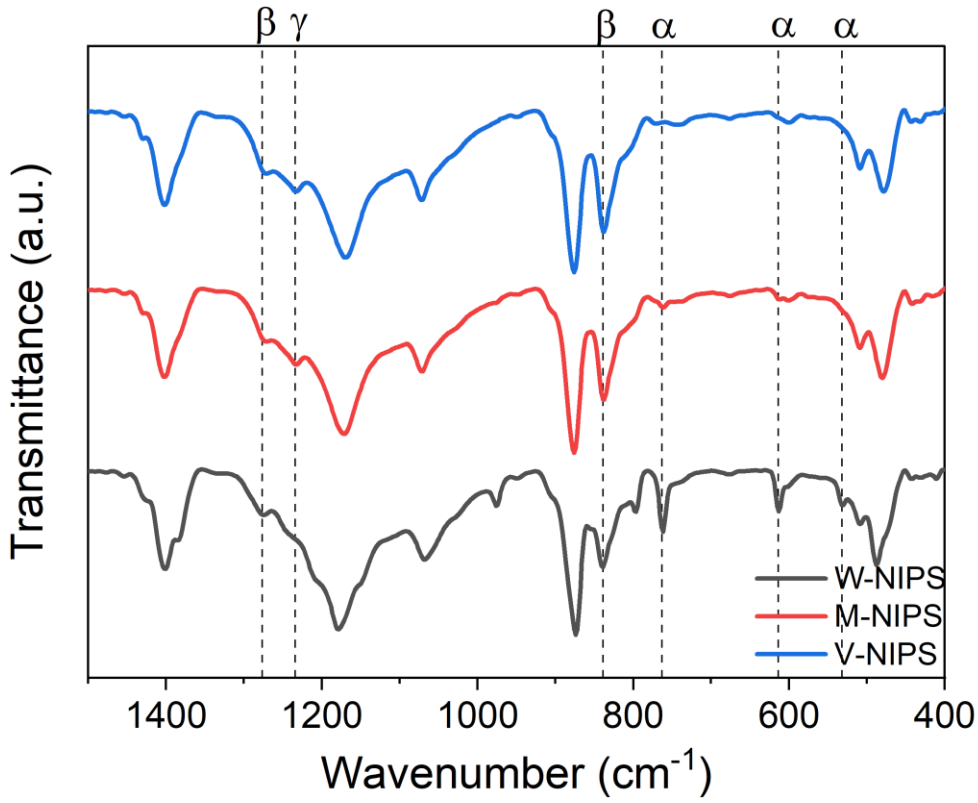

Fig. S1: ATR-FTIR transmittance spectra of W-NIPS, M-NIPS and V-NIPS membranes in the range of 1500 cm^{-1} to 400 cm^{-1}. The different crystalline polymorphs associated with different membranes prepared was assessed using ATR-FTIR. Crystalline phase in PVDF predominantly exists in α, β and γ phases[1]. From the transmittance spectrum, the α phase (763 cm^{-1}, 614 cm^{-1}, 532 cm^{-1}) which is also the kinetically favourable form is the dominant phase in W-NIPS while β and γ phases (β at 839 cm^{-1}, 1276 cm^{-1} and γ at 1234 cm^{-1}) dominate M-NIPS and V-NIPS[2]. Zhang and co-authors[3] note that a subcritical β phase (thermodynamically metastable) crystal embryo can either grow into a nucleus or redissolve in the liquid. As a result, delayed de-mixing (M-NIPS and V-NIPS) can allow for enhancement of the β phase as can been see from the peak at 839 cm^{-1}. Taken together, these results allow for indirect confirmation regarding the various modes of de-mixing governing W-NIPS, M-NIPS and V-NIPS.

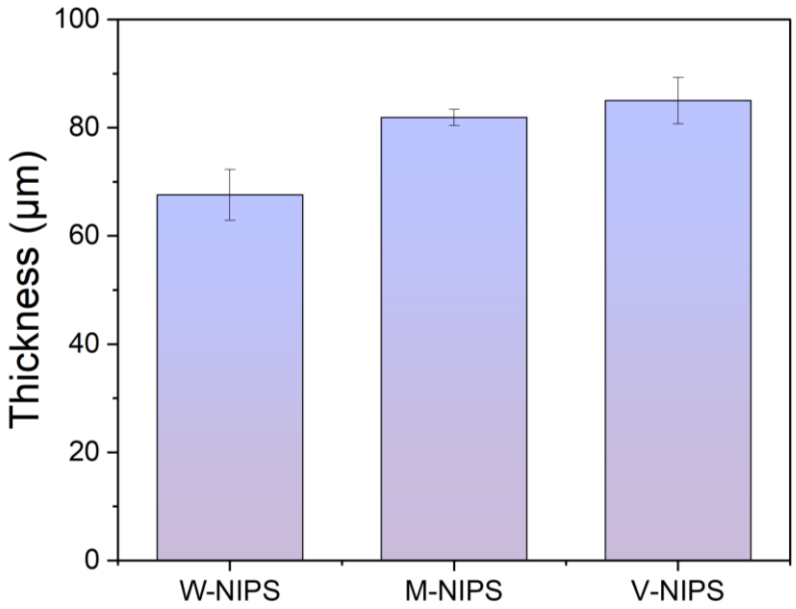

Fig. S2: Membrane thickness for different membranes. Variation in membrane thickness as estimated from cross-sectional SEM imaging for different fabrication routes.

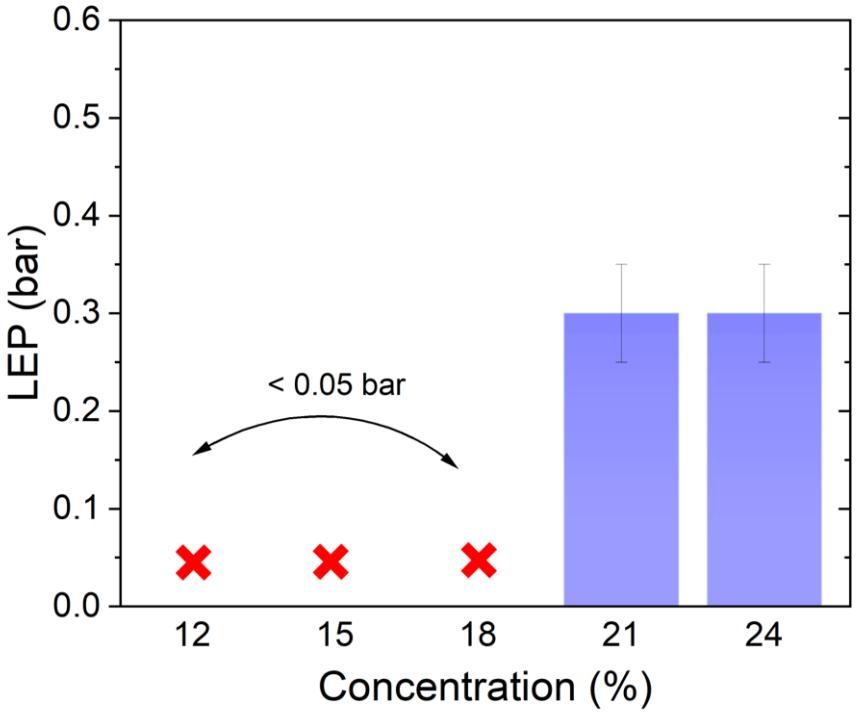

Fig. S3: Variation of Liquid Entry Pressure (LEP) for different polymer concentrations (in wt.%) for M-NIPS membranes. Red-cross symbol implies LEP was lower than 0.05 bar making them unsuitable for MD applications. Above 21 wt.% polymer concentration, there was no significant change in LEP.

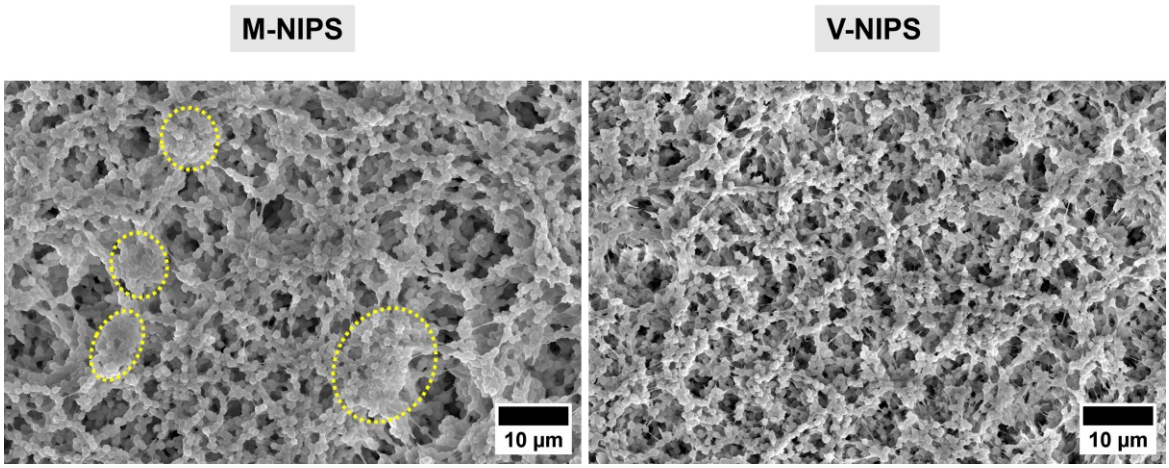

Fig. S4: Top surface SEM images comparing M-NIPS and V-NIPS. A comparison of the top membrane surface SEM images of M-NIPS and V-NIPS reveal isolated areas where PVDF polymer has agglomerated leading to large spherulitic features (yellow dotted circles) for M-NIPS while the latter exhibits uniformly interconnected porous morphology.

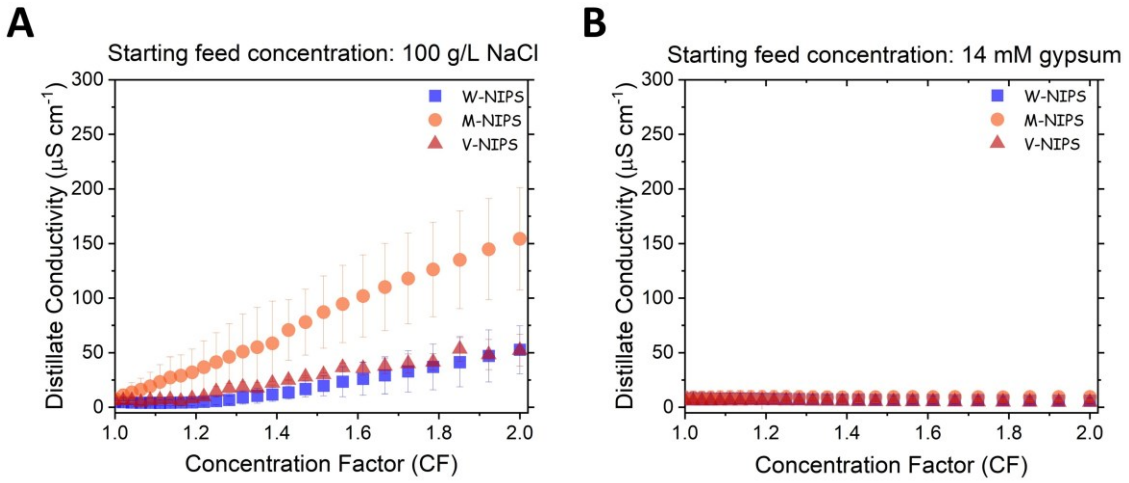

Fig. S5: Distillate tank conductivity profile with increase in feed concentration. Distillate tank conductivity vs. concentration factor (CF) when the starting feed concentration is **A** 100 g/L NaCl and **B** 14 mM gypsum. Error bars represent standard deviation arising from three independent membrane tests (n = 3).

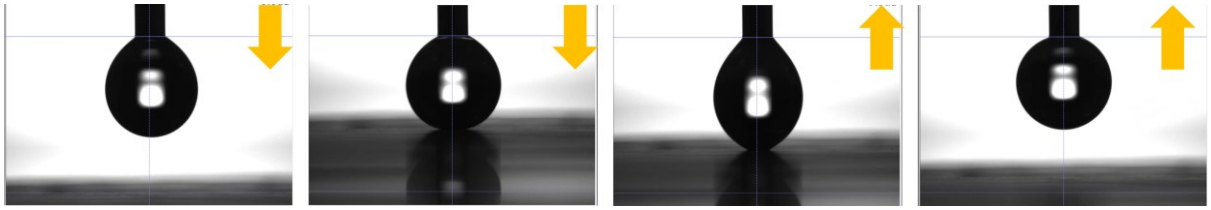

Fig. S6: Automatic dispenser attempting to deposit a 5 µL droplet on top of IPA-NIPS membrane. Yellow arrows indicate direction of needle/droplet movement.

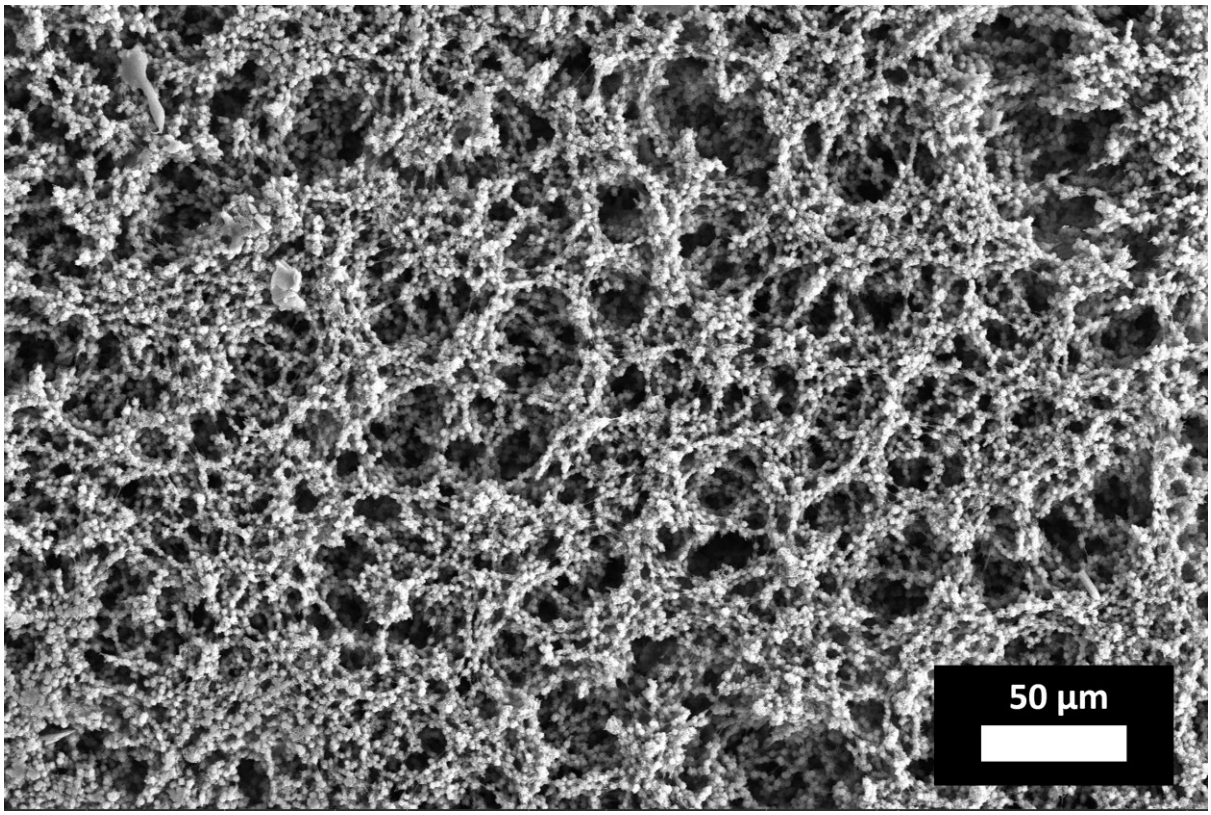

Fig. S7: Top surface FE-SEM image of IPA-NIPS membrane. IPA-NIPS featured a highly porous interconnected morphology similar to that of M-NIPS and V-NIPS.

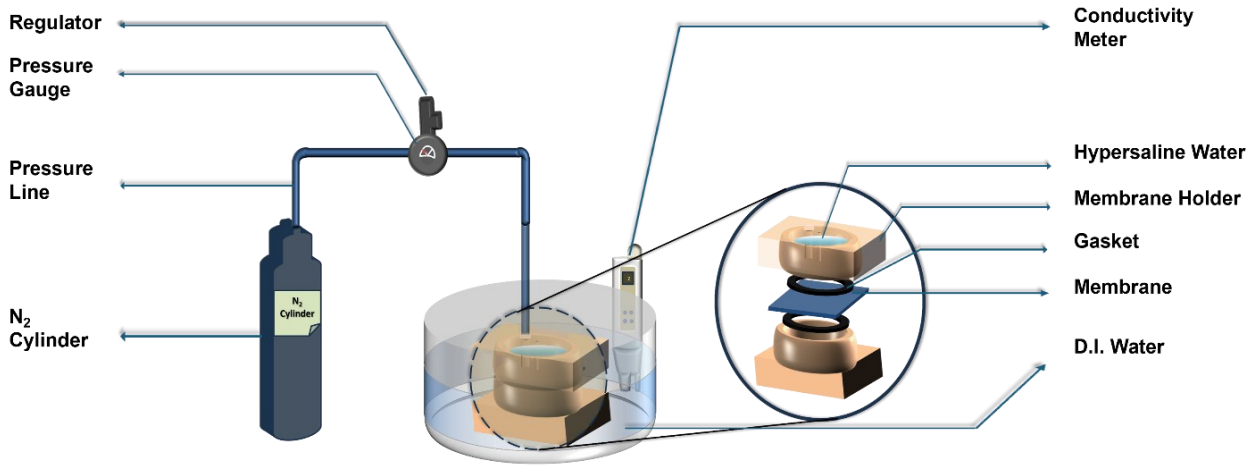

Figure S8. Schematic of liquid entry pressure (LEP) measurement setup. The membrane chamber (shown in the expanded view) is primarily composed of two chambers: the top and bottom. The top chamber has two inlets, one for air flow (pressurizing) and the other for dosing highly saline water that will rest on the top side of the membrane. The bottom chamber is hollow, allowing any trace of saline water that penetrates the membrane to flow through. Once the membrane is inserted and clamped between these two chambers, it is partially submerged in a bath containing water of very low conductivity. Water is filled in the bath such that it touches the bottom of the membrane housed in the membrane chamber. The instant at which the largest membrane pore is compromised, i.e. saline water penetrates the membrane bulk, a rise in conductivity is detected on the conductivity meter dipped in the bath. This is measured as the liquid entry pressure (LEP) of the membrane. A pressure regulator is used to control the pressure applied to the membrane surface. The whole setup, as shown, is placed on a magnetic stirrer with a magnetic bead placed in the hollow section of the bottom chamber so that there is no delay in detection of the LEP.

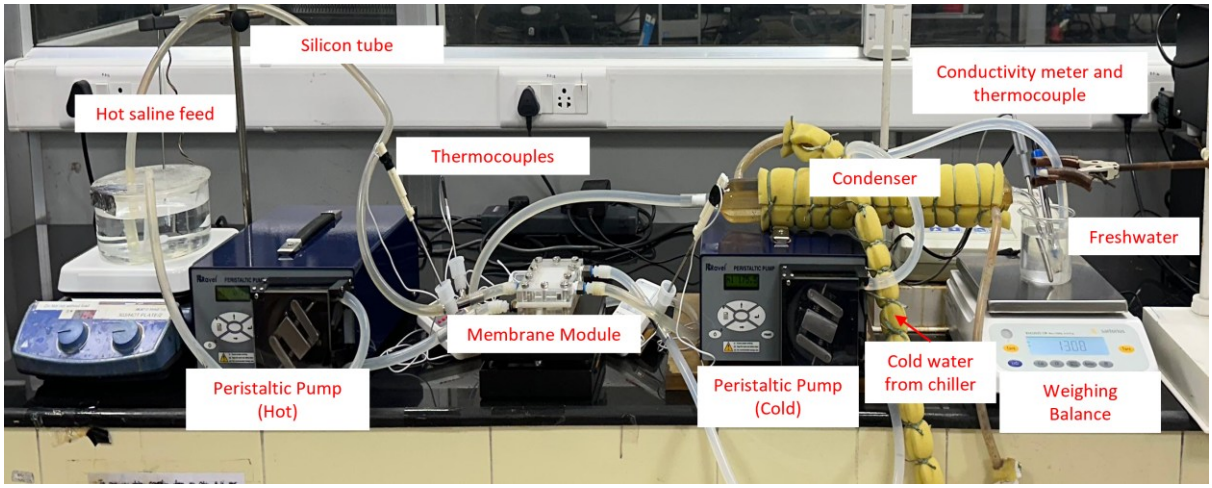

Figure S9. Membrane Distillation (MD) setup employed for carrying out hypersaline experiments. The DCMD module in our work consists of three parts – a hot side, a cold side, and a membrane module where the former two parts meet. Peristaltic pumps (RH-P100L, Ravel Hiteks Ltd.) are employed to circulate the hot saline feed and the cold freshwater. Temperature (METRAVI ST-9283B) and pressure (ITEC) probes are installed just at the inlet and outlet of the membrane module. A hot plate (IKA C-MAG HS 7) is used to heat the saline water, while at the cold end, a condenser with the aid of a chiller (Laboratory Chiller, LALCO Scientific Instruments) is used to cool the fresh water. Both the hot and cold streams are recirculated throughout via the peristaltic pumps. The freshwater beaker is placed on top of a weighing balance (PGB 6000, Wensar) so that the increment in water collected can be noted. A conductivity meter (Model 602, ESICO INTERNATIONAL) is dipped in the freshwater beaker at the cold side to detect the passage of any salts through the membrane. The membrane module is made up of transparent acrylic sheet and rubber gaskets are employed on both sides of the membrane to allow for a flow passage of 1.5 mm height for both hot and cold streams.

Text S1: **Details of calculations for evaluating the effect of adjusting permeate temperature on temperature polarization**

The following calculations were performed to understand the effect on temperature polarization when permeate temperature is adjusted for a fixed feed temperature.

To understand the extent up to which temperature polarization is affected by adjusting permeate temperature, we carried out MD experiments using 0.45C_PVDF at different permeate temperatures while attempting to keep the feed temperature constant with de-ionized water flowing on either side.

The following assumptions were made:

1. The bulk temperatures on the feed and permeate sides are approximated by the averages of their respective inlet and outlet temperatures. Similarly, the spatial variability of temperature polarization along the module length is assumed to be not significant. These axial variations are valid as the module length was short (L = 6.5 cm).
2. The thermal conductivity of the porous membrane is evaluated at the average of bulk temperatures of feed and permeate.
3. Heat loss to the ambient is assumed to be negligible.
4. Negligible concentration polarization occurred as no salt was present in the feed.

In the **Table S1** below, $T_{f,in}$ and $T_{f,out}$ refer to the feed inlet and feed outlet temperature measured just outside the membrane module and $T_{f,b}$ refers to the average of $T_{f,out}$ and $T_{f,out}$.

Similarly, $T_{p,in}$ and $T_{p,out}$ refers to the permeate inlet and permeate outlet temperature measured just outside the module and $T_{p,b}$ refers to the average of $T_{p,in}$ and $T_{p,out}$.

	$T_{f,in}$ (°C)	$T_{f,out}$ (°C)	$T_{f,b}$ (°C)	$T_{p,in}$ (°C)	$T_{p,out}$ (°C)	$T_{p,b}$ (°C)	Flux (LMH)
Experiment 1	61.3	59.8	60.6	22.2	24.5	23.4	21
Experiment 2	61.3	59.8	60.6	30	31.8	30.9	18.9
Experiment 3	61.5	60.2	60.9	35.5	37.1	36.6	15.3

Table S1: Inlet, outlet and bulk temperatures for feed and permeate side for three different experiments in which permeate temperature was adjusted while maintaining a fixed feed temperature and corresponding flux for each experiment. These values were collected after attaining steady state which is about 1 hour after the temperature stabilized.

Heat flux through the thermal boundary layer (Q_f) at the feed side can be estimated as,

$$Q_f = h_f\,(T_{f,b} - T_{f,m})$$ ----------(S1)

Where h_f is the convective heat transfer at feed-membrane interface and can be calculated using the Sider-Tate correlation[4] for Nusselt number (Nu_f) as

$$Nu_f = 1.86 * \left(\frac{Re*Pr}{\frac{L}{D_H}}\right)^{1/3}$$ ----------(S2)

and $h_f = \frac{Nu_f * k_{fluid}}{D_H}$ ----------(S3)

where Re and Pr are the Reynold's number and Prandtl number on the feed side, respectively, L is the length of the feed channel (6.5 cm), k_{fluid} is the thermal conductivity of water (W m^{-1} K^{-1}) evaluated at different temperatures[5] and D_H is the hydraulic diameter of the feed channel estimated as

$$D_H = \frac{2wh}{w+h}$$ ----------(S4)

where w and h are the width (3.1 cm) and height of the feed channel (3 mm), respectively.

At the same time the total heat flux through the membrane is,

$$Q_m = \frac{k_m}{\delta_m}\left(T_{f,m} - T_{p,m}\right) + J_V H_V$$ ----------(S5)

$$k_m = \epsilon k_{air} + (1-\epsilon) k_{PVDF}$$ ----------(S6)

where k_m refers to membrane thermal conductivity (W $m^{-1}K^{-1}$), ϵ refers to membrane porosity (0.7), k_{air} and k_{PVDF} refers to thermal conductivity of air and PVDF (W $m^{-1}K^{-1}$) respectively and this was calculated using correlations provided by Ibrahim and Alsalhy[6] and Lawson and Lloyd[7], δ_m refers to membrane thickness (m), J_V refers to water vapour condensed (kg m^{-2} s^{-1}) and H_V refers to the latent heat of vaporization (J kg^{-1}).

Heat flux through the thermal boundary layer on the permeate side can be written in a similar way as that of the feed side:

$$Q_p = h_p\,(T_{p,m} - T_{p,b})$$ ----------(S7)

At steady state,

$$Q_f = Q_m = Q_p$$ ---------- (S8)

i.e.

$$h_f\left(T_{f,b} - T_{f,m}\right) = \frac{k_m}{\delta_m}\left(T_{f,m} - T_{p,m}\right) + J_V H_V = h_p\,(T_{p,m} - T_{p,b})$$ ----------(S9)

Solving the above equation for each experiment allows us to estimate the interfacial temperatures and temperature polarization coefficient (TPC) as listed in the **Table S2** below:

	$T_{f,b}$ (°C)	$T_{p,b}$ (°C)	$T_{f,m}$ (°C)	$T_{p,m}$ (°C)	TPC
Experiment 1	60.6	23.4	49.5	35.5	0.38
Experiment 2	60.6	30.9	51.3	40.9	0.35
Experiment 3	60.9	36.3	53.3	44.5	0.36

Table S2: **Temperatures evaluated at the feed and permeate interfaces and corresponding TPC values**.

where TPC is estimated as

$$TPC = \frac{T_{f,m} - T_{p,m}}{T_{f,b} - T_{p,b}}$$ ---------- (S10)

Note: temperature dependent physical parameters such as (viscosity) and (density) was evaluated from Huber et al[8].

TPC values (Table S2) for different permeate temperatures suggest that adjusting the permeate temperature may not influence temperature polarization significantly. Manawi et al.[9] also noted a similar phenomenon where TPC changed by only about 0.03 upon going from 60-20°C to 60-30°C.

Representative calculations for **Experiment 1** are listed in **Table S3**:

Parameter	Feed	Permeate
Density, ρ_w	984 kg m^{-3}	998 kg m^{-3}
Velocity, v	0.143 m/s	0.116 m/s

Hydraulic diameter, D_H	$\frac{2*w*h}{w+h} = \frac{2*0.031*0.003}{0.031+0.003} = 0.0054$ m	
Dynamic viscosity, μ_w	$4.66 * 10^{-4}$ Pa s	$0.9 * 10^{-3}$ Pa s
Heat capacity, Cp_w	4185 J kg^{-1} K^{-1}	4180 J kg^{-1} K^{-1}
Thermal conductivity of water, k_w	0.641 W m^{-1} K^{-1}	0.605 W m^{-1} K^{-1}
Re	1630.6	694.6
Pr	3.04	6.21
L/D_H	$0.065/0.0054 = 12$	
Nu	13.6	13.2
h_f	1614.4 W m^{-2} K^{-1}	1481.1 W m^{-2} K^{-1}
$h_{f\,(modified)}$*	2098.72 W m^{-2} K^{-1}	1925.5 W m^{-2} K^{-1}
k_m (evaluated at 42.3°C)	0.0759 W m^{-1} K^{-1}	
k_m/δ_m	$\frac{0.0759\ (W\ m^{-1}K^{-1})}{110 * 10^{-6}\ (m)} = 690$	
$J_v * \Delta H_v$	13536 W m^{-2}	

Table S3: Sample calculations carried out to assess TPC value for experiment 1.

*Heat transfer coefficient for both feed and permeate side were multiplied with a correction factor of 1.3 to account for turbulent effects at the inlet and outlet of the feed and permeate channel since the membrane module was small in size[10] (total length of feed channel was 6.5 cm and width was 3.1 cm).

Resulting two equations are:

$$2098.7\ (60.6 - T_{f,m}) = 690\ (T_{f,m} - T_{p,m}) + 13536 \quad \text{---------- (S11)}$$

$$13536 + 690\ (T_{f,m} - T_{p,m}) = 1925.5\ (T_{p,m} - 23.4) \quad \text{---------- (S12)}$$

These equations are solved simultaneously to get $T_{f,m} = 49.5°C$ and $T_{f,m} = 35.5°C$.

Supplementary Movie 1: Real-time visualization of water droplets moving over W-NIPS, M-NIPS and V-NIPS

References

1 Cai, X., Lei, T., Sun, D. & Lin, L. A critical analysis of the α, β and γ phases in poly(vinylidene fluoride) using FTIR. *RSC Advances* **7**, 15382-15389 (2017). https://doi.org/10.1039/C7RA01267E

2 Cui, Z., Hassankiadeh, N. T., Zhuang, Y., Drioli, E. & Lee, Y. M. Crystalline polymorphism in poly(vinylidenefluoride) membranes. *Progress in Polymer*

Science **51**, 94-126 (2015). https://doi.org/https://doi.org/10.1016/j.progpolymsci.2015.07.007

3 Zhang, M., Zhang, A.-Q., Zhu, B.-K., Du, C.-H. & Xu, Y.-Y. Polymorphism in porous poly(vinylidene fluoride) membranes formed via immersion precipitation process. *Journal of Membrane Science* **319**, 169-175 (2008). https://doi.org/https://doi.org/10.1016/j.memsci.2008.03.029

4 Sieder, E. N. & Tate, G. E. Heat Transfer and Pressure Drop of Liquids in Tubes. *Industrial & Engineering Chemistry* **28**, 1429-1435 (1936). https://doi.org/10.1021/ie50324a027

5 Ramires, M. L. V. *et al.* Standard Reference Data for the Thermal Conductivity of Water. *Journal of Physical and Chemical Reference Data* **24**, 1377-1381 (1995). https://doi.org/10.1063/1.555963

6 Ibrahim, S. S. & Alsalhy, Q. F. Modeling and simulation for direct contact membrane distillation in hollow fiber modules. *AIChE Journal* **59**, 589-603 (2013). https://doi.org/https://doi.org/10.1002/aic.13845

7 Lawson, K. W. & Lloyd, D. R. Membrane distillation. *Journal of Membrane Science* **124**, 1-25 (1997). https://doi.org/https://doi.org/10.1016/S0376-7388(96)00236-0

8 Huber, M. L. *et al.* New International Formulation for the Viscosity of H2O. *Journal of Physical and Chemical Reference Data* **38**, 101-125 (2009). https://doi.org/10.1063/1.3088050

9 Manawi, Y. M., Khraisheh, M. A. M. M., Fard, A. K., Benyahia, F. & Adham, S. A predictive model for the assessment of the temperature polarization effect in direct contact membrane distillation desalination of high salinity feed. *Desalination* **341**, 38-49 (2014). https://doi.org/https://doi.org/10.1016/j.desal.2014.02.028

10 Hijaz, H. A., Zargar, M., Shafieian, A., Razmjou, A. & Khiadani, M. Experimental investigation of temperature polarisation by capturing the temperature profile development over DCMD membranes. *Journal of Membrane Science* **687**, 122089 (2023). https://doi.org/https://doi.org/10.1016/j.memsci.2023.122089